Desalination and Water Treatment
www.deswater.com

doi: 10.5004/dwt.2022.28600

266 (2022) 236–246
August

Adsorption behavior and mechanism of atrazine on biochar obtained from the peanut shell

Siwei Qiu[a], Xiangjuan Yuan[a], Lei Sun[a,*], Dongsheng Xia[a,b,*]

[a]*School of Environmental Engineering, Wuhan Textile University, Wuhan 430073, China, Tel. +86 27 59367685; Fax +86 27 59367338; emails: sunlei@wtu.edu.cn (L. Sun), dongsheng_xia@wtu.edu.cn (D.S. Xia), channdy.qiu@gmail.com (S.W. Qiu), yuanxiangjuan1986@outlook.com (X.J. Yuan)*
[b]*Engineering Research Center for Clean Production of Textile Dyeing and Printing, Ministry of Education, Wuhan 430073, China*

Received 4 January 2022; Accepted 4 June 2022

ABSTRACT

A series of peanut shell (PS) based biochar were prepared by the direct pyrolysis (BPS) and subsequent hydrothermal treatment procedures with water (HPS) and potassium carbonate (K_2CO_3) (KPS). The obtained PS-based biochars were applied as the effective adsorbents to remove atrazine (ATZ) in aqueous solution. The characterization analysis demonstrated that the PS-based biochar treated with KPS had large specific surface area (335.27 m^2 g^{-1}), abundant pore structure and surface functional groups. The results show that 98% of ATZ removal efficiency within 3 h was achieved in the KPS-adsorption process and the maximal adsorption (Q_m) of ATZ adsorption was 11.78 mg g^{-1}. Besides, the effects of dosage, initial concentration, and solution pH on ATZ adsorption were systematically evaluated. Moreover, the regeneration ability of KPS was evaluated through cycle trial. Furthermore, the isotherms, kinetics and thermodynamic of the PS-based biochar on ATZ adsorption were also explored. The results demonstrated that the ATZ adsorption followed the pseudo-second-order kinetics model, and the Freundlich isotherm model was able to adequately describe the adsorption on ATZ. In conclusion, the PS-based biochar modified by K_2CO_3 hydrothermal treatment can be used as an efficient adsorbent for the removal of ATZ from wastewater.

Keywords: Adsorption; Atrazine; Biochar; Hydrothermal modification; Peanut shell

1. Introduction

Atrazine (ATZ), one of the most widely used chemical herbicides, is a triazine herbicide that has been widely used to control annual grasses and broadleaf weeds in agricultural settings [1]. The ways of ATZ entering into the environment mainly include precipitation, run-off, and leaching. Unfortunately, the persistence, moderate aqueous solubility, high mobility, long half-life, and difficult biodegradation ability of ATZ have made its elimination relatively inefficient in wastewater [2]. In addition, ATZ was also classified as an endocrine disruptor that affects the central nervous, endocrine and immune systems [3]. ATZ with concentration over 3 mg L^{-1} could damage animal reproductive system and even pose a potential threat to human health [4]. Therefore, it is of vital importance to seek efficient treatment technology to remove ATZ from aquatic environment and farmland soil.

At present, the adsorption, photo catalysis, biodegradation and other treatment technologies have been widely developed and applied for ATZ removal [5]. Amongst, the adsorption is the key factor to control the migration, transformation, orientation and bioavailability of ATZ in the environment, which could directly affect the treatment efficiency of ATZ [6]. For now, activated carbon and biochar have been the most commonly used adsorbents for ATZ removal. Noteworthy, biochar is a highly aromatic

* Corresponding authors.

carbon-rich material produced by the pyrolysis of biomass raw materials under oxygen-limited conditions. The great specific surface area of biochar could provide sorption sites for contaminants, then the rich surface functional groups, aromaticity, and negative surface charge of biochar may increase the sorption capacity via electron donor-acceptor interaction, hydrogen bonding, hydrophobic binding, and electrostatic effects [7]. In comparison with activated carbon, biochar with the wide raw material sources and relatively low cost, has been attracted considerable attentions in water treatment.

Peanuts are one of the common and important crops in China. The use of peanut shell (PS) as raw material for biochar preparation would be environmentally friendly and economically feasible, which can further realize the resource recovery of agricultural waste and reduce the waste disposal [8]. Nowadays, PS-based biochar has been widely used, such as adsorbents to remove heavy metals [9] and organic contaminants [10], and catalysts for Fenton [11], catalytic ozonation [12] and peroxymonosulfate/persulfate activation processes, etc. [13,14]. Yokley and Cheung [15] reported that the PS-based biochar under the pyrolysis temperature of 600°C exhibited higher adsorption capacity of ATZ than the PS-based biochar calcinated at 300°C. Xu et al. [16] found that the nitrogen and sulfur doped PS has greatly enhanced adsorption capacity for diethyl phthalate (DEP) and the maximum adsorption capacity for DEP could reach 14.34 mg g^{-1}. Liu et al. [17] investigated that the PS activated by ammonium polyphosphate showed excellent adsorption performance with a monolayer chloramphenicol adsorption capacity up to 423.7 mg g^{-1}. At present, a number of researchers have tried to improve the adsorption capacity of PS-based biochar via the surface modification and structural doping methods. Nevertheless, the effects of the hydrothermal modification on the adsorption performance of PS-based biochar have been rarely reported.

In this study, a series of the PS-based biochar were synthesized via the hydrothermal activation methods. The obtained PS-based biochars were applied as the effective adsorbents to remove ATZ in aqueous solution. Several characterizations were performed to investigate the physicochemical properties of the obtained biochar. In addition, the adsorption properties of the biochars and the influences of pH, dosage and temperature on ATZ adsorption were further studied. Moreover, the equilibrium and kinetics studies were also performed to optimize and evaluate the adsorption behavior of ATZ by the modified biochar. The objectives were (1) to assess how modification method affected the adsorption of ATZ onto biochars, (2) to explore the effects of adsorption conditions and adsorption behaviour on the adsorption of ATZ onto biochars, and (3) to elucidate the mechanism underlying the adsorption of ATZ onto biochars.

2. Materials and methods

2.1. Chemicals and reagents

All chemicals and solvents used were at least in analytical grade without further purification, and as received from various commercial suppliers. K_2CO_3, sodium hydroxide (NaOH), hydrochloric acid (HCl), and ethyl acetate of analytical grade were supplied by Sinopharm Chemical Reagent (China). ATZ with the highest purity available (>97%) was provided by TCI Chemicals, Japan. Ultrapure water (>18.2 MΩ·cm) obtained from a Millipore Milli-Q system (A10, Millipore, USA) was used for all the synthesis and treatment.

2.2. Preparation of the PS-based biochar

PS, which was collected from Henan Province (China), was rinsed with deionized water to remove surface dirt. The shell was air dried (to constant mass), milled by a high-speed smashing machine, and then passed through an 80-mesh sieve. 10 g PS was pyrolyzed with a quartz boat in the tubular furnace under a continuous flow of N_2 and heated to 700°C for 2 h with a heating rate of 5°C min^{-1}. After cooling to room temperature and passing 80-mesh sieve, the biochar (BPS, which refers to the biochar directly prepared from peanut shell) was obtained for subsequent characterization analysis and batch adsorption experiment.

The modified biochar was prepared from peanut shell by hydrothermal method with K_2CO_3 and H_2O, respectively. Among them, HPS refers to the biochar prepared from peanut shell after water activation, and KPS refers to the peanut shell biochar material prepared after potassium carbonate modification. 1 g PS mixed with 30 mL K_2CO_3 (0.1 M), in the high-pressure kettle, further heated to 120°C for 24 h with a heating rate of 5°C min^{-1}. The final resultant was washed several times with pure water and then was dried for 6 h in a vacuum hot air oven at 80°C, which was denoted as KPS (KPS refers to the peanut shell biochar material prepared after potassium carbonate modification). Moreover, the same method was carried out to obtain HPS by substitute the K_2CO_3 solution by ultrapure water (HPS refers to the biochar prepared from peanut shell after water activation).

2.3. Characterization

Scanning electron microscopy (SEM) was undertaken to observe structural morphology (FEG 250, Quanta, USA). The Brunauer–Emmett–Teller (BET) surface area of the biochar was determined by a Micromeritics ASAP 2460 Porosimeter (USA). The X-ray diffraction (XRD) patterns were recorded on a PANalytical X'Pert Pro MPD X-ray Diffractometer (Netherlands) with Cu Kα radiation (λ = 0.154178 nm). Fourier-transform infrared (FT-IR) analysis was carried out using KBr in the range 400–4,000 cm^{-1} (Nicolet iS5, Thermo Scientific, USA). X-ray photoelectron spectroscopy (XPS) measurements were performed on a Thermo Scientific ESCALAB 250Xi system (USA). (Specific information: the vacuum of the analysis room is $8 \times l0^{-10}$ Pa, the excitation source is Alka ray (HV = 1486.6 eV), the working voltage is 12.5 kV, and the filament current is 16 mA. Meanwhile, charge correction was carried out according to C 1s = 284.80 eV combined with energy standard when the step size was set at 0.05 eV and residence time was 40–50 ms during the test).

2.4. Adsorption experiments

Batch adsorption experiments were conducted in the 250 mL conical flasks on the magnetic stirring apparatus and the solution temperature was maintained at 30°C. The

sorption kinetic experiments were conducted in 100 mL of 5 mg L^{-1} ATZ solution. The dosage effect experiments of the PS-based biochar were carried out at dosage range from 10 to 100 mg L^{-1}. The pH effect experiments were conducted in pH range from 3 to 10. The sorption isotherm experiments were conducted with initial ATZ concentrations from 1 to 10 mg L^{-1} for 3 h adsorption, and the thermodynamics experiments were carried out at between 20°C and 40°C. Each of these variables was tested respectively, and all the experiments were carried out for 3 h.

During the reaction, the samples were taken interval and immediately filtered through the 0.45 μm film and subjected to centrifugation at 10000 rpm for 10 min. The ATZ was extracted with the ethyl acetate at the volume ratio of 1:1, and the extract solution were determined by Gas Chromatograph with Electron Capture Detector (GC-ECD, 7890B-5977, Agilent Technologies, USA) for ATZ concentration analysis [18]. Ethyl acetate was used as extraction agent, and the column temperature was kept at 75°C for 0.5 min at 10°C /min and increased from 75°C to 300°C for 2 min at 300°C. Helium and nitrogen were used as carrier gas and tail gas at flow rates of 1.0 and 30 mL min^{-1}, respectively. The samples were detected by μECD detector at 350°C with an injection volume of 40 μL. The equilibrium adsorption capacity, Q_e (mg g^{-1}) and the removal efficiency were calculated using the following formulae:

$$Q_e = \frac{(C_0 - C_e)V}{m} \quad (1)$$

where C_0 and C_e are the initial concentration of ATZ mg L^{-1} and equilibrium concentration of ATZ mg L^{-1}, V = volume of the ATZ solution (L), and m is the mass of the PS-based biochar (g). The Q_e represented the amount of adsorbed ATZ per gram adsorbent at equilibrium (mg g^{-1}).

3. Results and discussion

3.1. Characterizations of BPS, KPS and HPS biochar

The specific surface area and pore distribution of the different PS-based biochar were determined by the N_2 adsorption–desorption measurement and the results were displayed in Fig. 1. As shown in Fig. 1, the adsorption isotherms of BPS, HPS and KPS were similar, and displayed

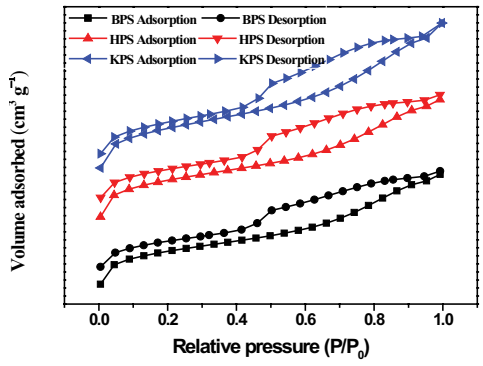

Fig. 1. N_2 adsorption–desorption isotherms of the PS-based biochar.

the type IV hysteresis behavior, indicating the presence of mesoporous-structure [19]. The main mesoporous structure may provide more active sites for pollutants removal [20]. As represented in Table 1, the BET specific surface area of BPS was 307.17 m^2 g^{-1}. The pore size and volume of BPS were 29.11 Å and 0.23 cm^3 g^{-1}, respectively. The biochar modified by the hydrothermal method had obviously enhanced on the BET specific surface area, pore size, and pore volume. Moreover, the KPS had the largest BET specific surface area, which could reach 335.27 m^2 g^{-1}. The pore size and volume of KPS respectively were 30.48 Å and 0.26 cm^3 g^{-1}. It was indicated that the large specific surface in KPS could be beneficial for the adsorption, desorption and diffusion of reactants and products, further greatly accelerating the ATZ removel [21]. Kim et al. also reported that using K_2CO_3 as an activation agent can increase the specific surface area and pore size of spent coffee ground-based microporous carbons material [22].

The surface morphology and structure of the PS-based biochar were investigated by the SEM characterization (Fig. 2). As shown in Fig. 2a and b, the BPS appeared a typical hardwood structure, supported by fiber cells, wood rays, and large pores, probably due to the degradation and destruction of cellulose and lignin [23]. The SEM image of HPS in Fig. 2c presents a towel crease structure with relatively smooth surface, which was attributed to the internal collapse and structural defects. On this basis, the KPS consisted of irregular flakes and pores in Fig. 2d, probably due to that the activation by K_2CO_3 can dramatically improve the degree of graphitization and the specific surface [24]. Moreover, the sylvite activators have higher etching efficiency, which are more likely to form microporous structures with low torque and good connectivity [25]. The specific surface area and pore size of KPS were clearly improved, which was consistent with the results of BET characterization Table 1.

The XRD patterns of BPS, HPS and KPS are illustrated in Fig. 3a. As exhibited in Fig. 3a, the PS-based biochars represented an obvious diffraction peak at 22.6°, which was the characteristic peak of cellulose crystal structure [26], indicating the presence of amorphous organic components. The characteristic peak at 29° of biochar reflects the graphitization degree of the material. After the hydrothermal treatment (KPS and HPS), the carbon structure still developed order, indicating the formation of crystalline materials. In addition, the crystal peak at 29° disappeared after the adsorption reaction, indicating that the adsorption changed the biochar. Some crystals in the material could generate the soluble compounds during the adsorption reaction, most of which could be further removed, thus obtaining no obvious crystal peak spectra [27].

Table 1
Pore structure parameters of three biomass carbon materials

Biochar	BET specific surface area (m^2 g^{-1})	Pore volume (cm^3 g^{-1})	Pore size (Å)
BPS	307.17	0.23	28.84
HPS	331.62	0.24	29.11
KPS	335.27	0.26	30.48

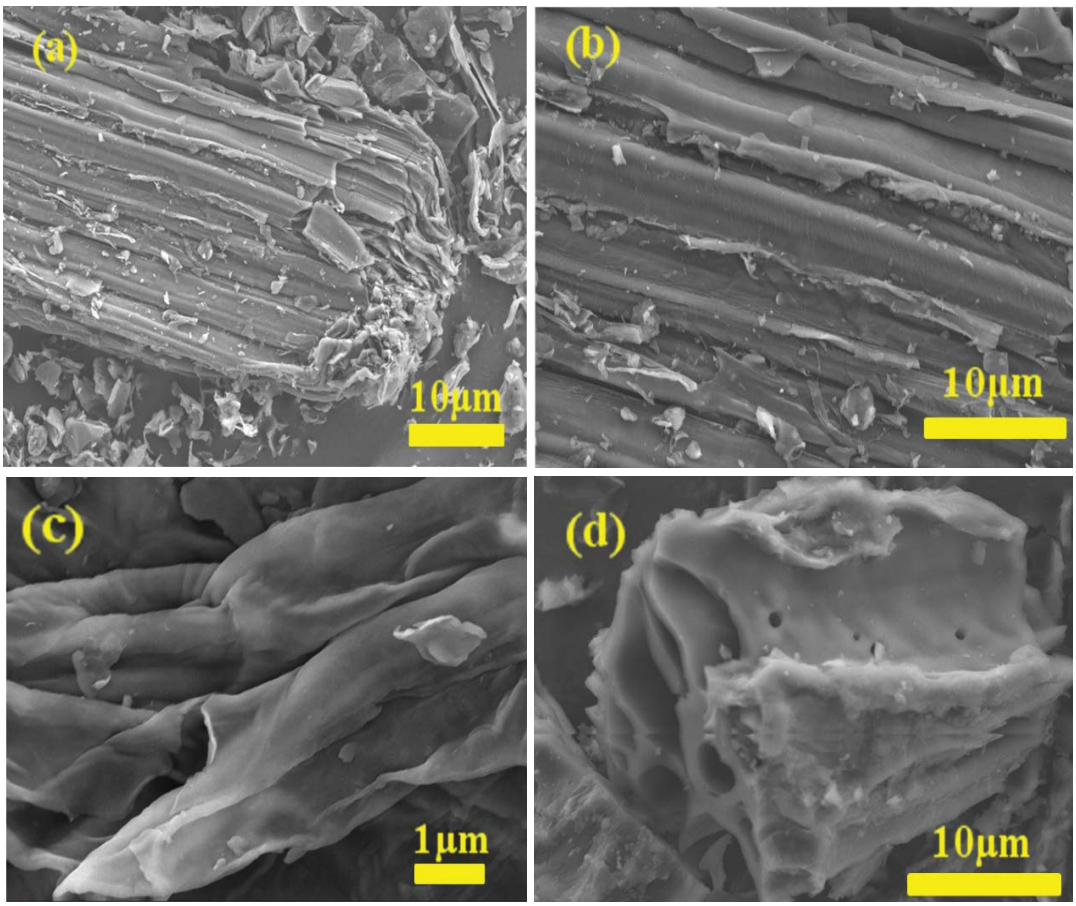

Fig. 2. SEM morphology of BPS (a, b), HPS (c), and KPS (d).

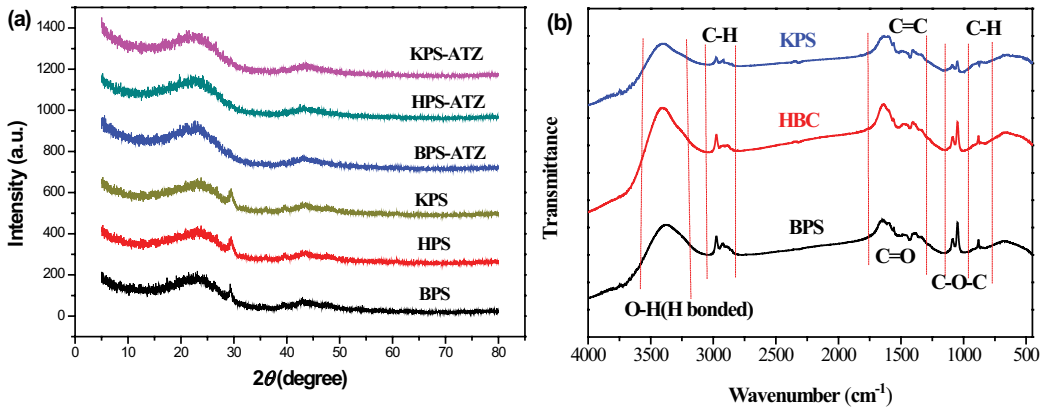

Fig. 3. XRD patterns (a), and FT-IR spectra (b) of the different PS-based biochar.

FT-IR spectra analysis was used to identify the chemical functional groups of the PS-based biochar (Fig. 3b). In the case of the PS-based biochar, the peak at about 3,400 cm^{-1} was ascribed to the stretching vibration of –OH groups [28]. The appearance of aromatic C–H bands (2,945 ~ 2,916 cm^{-1} and 885 ~ 750 cm^{-1}) and CH_3 (2,843 ~ 2,841 cm^{-1}) indicated greater aromatic fractions and greater degree of carbonization [29]. The decrease of KPS energy band may be caused by the fracture of C and H weak bonds of alkyl groups. It is speculated that K_2CO_3 could destroy the aromatic structure of PS-based biochar during activation process. Meanwhile, the absorption peak at 1,650 ~ 1,300 cm^{-1} were characteristic of aromatic C=O, C=C and C–C bonds [23]. The bands at 1,100 ~ 1,000 cm^{-1} were attributed to the alcohol C–O–C of cellulose.

In order to explore the chemical properties of the PS-based biochar, the characteristic peaks of C 1s and O 1s in XPS spectrum were analyzed. As shown in Fig. 4, the

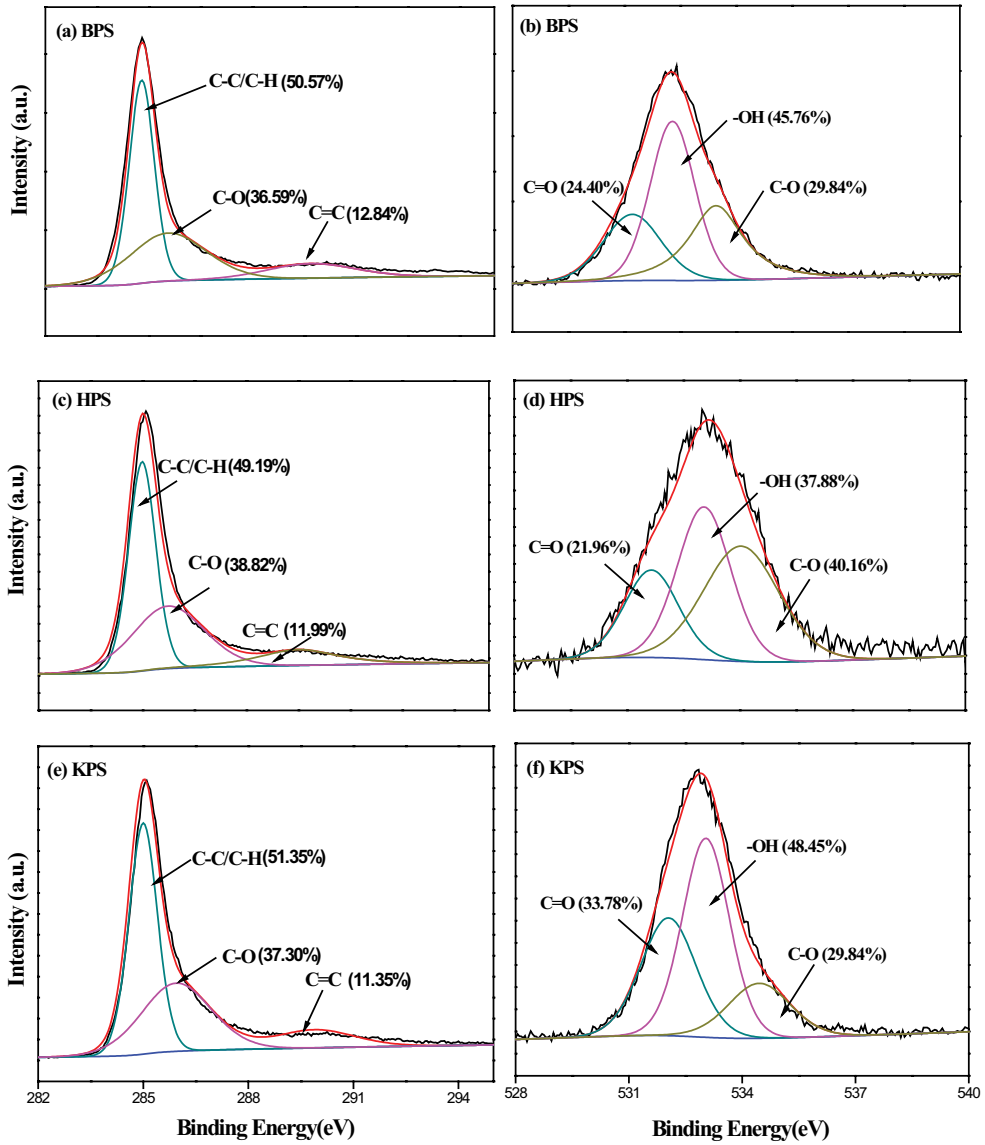

Fig. 4. High-resolution XPS spectra of the PS-based biochar and their fits in (a, c, e) C 1s, and (b, d, f) O 1s.

high-resolution C 1s spectrum of different PS-based biochar could be deconvolved into three peaks, namely, C–H/C–C (284.5 eV) [30], C–O (285.5–285.8 eV) [31], and C=C (287.8–290.5 eV) [29], respectively. Meanwhile, O 1s spectrum could be divided into two peaks, namely C=O (530.9~531.4 eV) [30], –OH (532.4~532.7 eV) and C–O (532.8–533.2 eV) [31]. The results demonstrated that the PS-based biochar had abundant surface functional groups, which were consistent with the previous FT-IR characterization. Furthermore, the C–C/C–H and C=O of the KPS increased and were more than the BPS and the C=C was decreased, due to destruction of aromatic structure by K_2CO_3.

Above all, the adsorption capacity of the PS-based biochar to organic pollutants was influenced by the physicochemical properties of biochar, such as polarity, such as polarity, aromaticity, specific surface area and pore volume. Of course, the physical and chemical properties of biochar materials prepared from peanut shell materials from different habitats may be influenced. During the activation of the biochar, K_2CO_3 would decompose into K_2O and CO_2 and the carbon atoms in lignin structure could react with K_2O to form potassium atoms, which would be conducive to the formation of micropores. Meanwhile, the redox reaction between K_2O and carbon atoms could also cause the structural defects leading to increase the specific surface area. The expansion and transfer of potassium atoms between the carbon layers are favorable for the formation of mesoporous and macropores [27]. Furthermore, the process of biochar adsorption was also accompanied by changes in the active groups.

3.2. Adsorption equilibrium of ATZ

The effect of the adsorption time on the adsorption performance of the PS-based biochar is shown in Fig. 5. With the increase of the adsorption time, the adsorption rate

increases rapidly at first and the ATZ adsorption reached equilibrium at around 30 min. The adsorption trend of the PS-based biochar to ATZ is roughly the same with the same pollutant concentration, showing three stages of "fast adsorption-slow adsorption–adsorption equilibrium", which basically reaches the equilibrium within 3 h. The removal efficiency of KPS on ATZ was significantly higher than the two biochar (BPS and HPS), and the saturated adsorption capacity could reach 11.7786 mg g^{-1}. Therefore, the larger specific surface area of the KPS provides more adsorption sites, and ATZ was removed under the combination of physical adsorption and chemical adsorption.

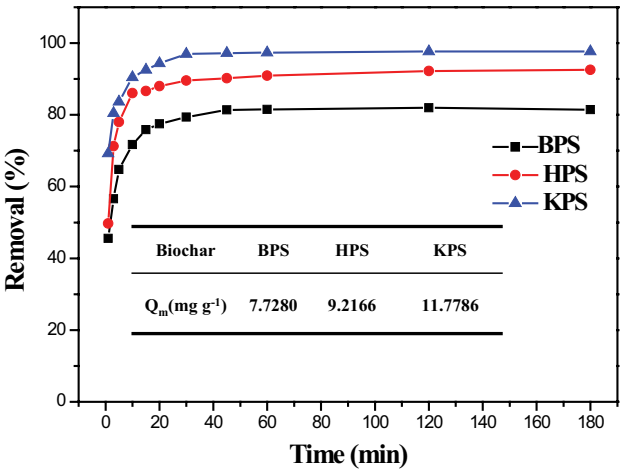

Fig. 5. The adsorption equilibrium of the PS-based biochar as a function of contact time. Experimental conditions: $[ATZ]_0$ = 5 mg L^{-1}; [biochar] = 500 mg L^{-1}; pH_0 = 7 ± 0.1.

3.3. Influence of experimental parameters for ATZ adsorption

3.3.1. KPS dosage

The effect of biochar dosage on the ATZ adsorption by KPS is depicted in Fig. 6a. When the biochar dosage increased from 0.01 to 0.05 g L^{-1}, the removal rate of ATZ by KPS significantly increased from 58.48% to 97.57%. The increased removal rate could be attributed to the increase of biochar, which not only increases the effective specific surface area of adsorption, but also increases the active site of adsorption [32]. Subsequently, the biochar dosage raised from 0.05 to 0.1 g L^{-1}, and the removal rate of ATZ remained unchanged. At the same time, the unit adsorption of ATZ by KPS decreased gradually with the variation of the dosage (Fig. 6a). In the case of limited solutes, excessive adsorbents would not only compete for solutes, but also overlap the effective adsorption active sites on the biochar surface.

3.3.2. Initial ATZ concentration

The effect of initial ATZ concentration on the ATZ adsorption by KPS is represented in Fig. 6b. With the increase of

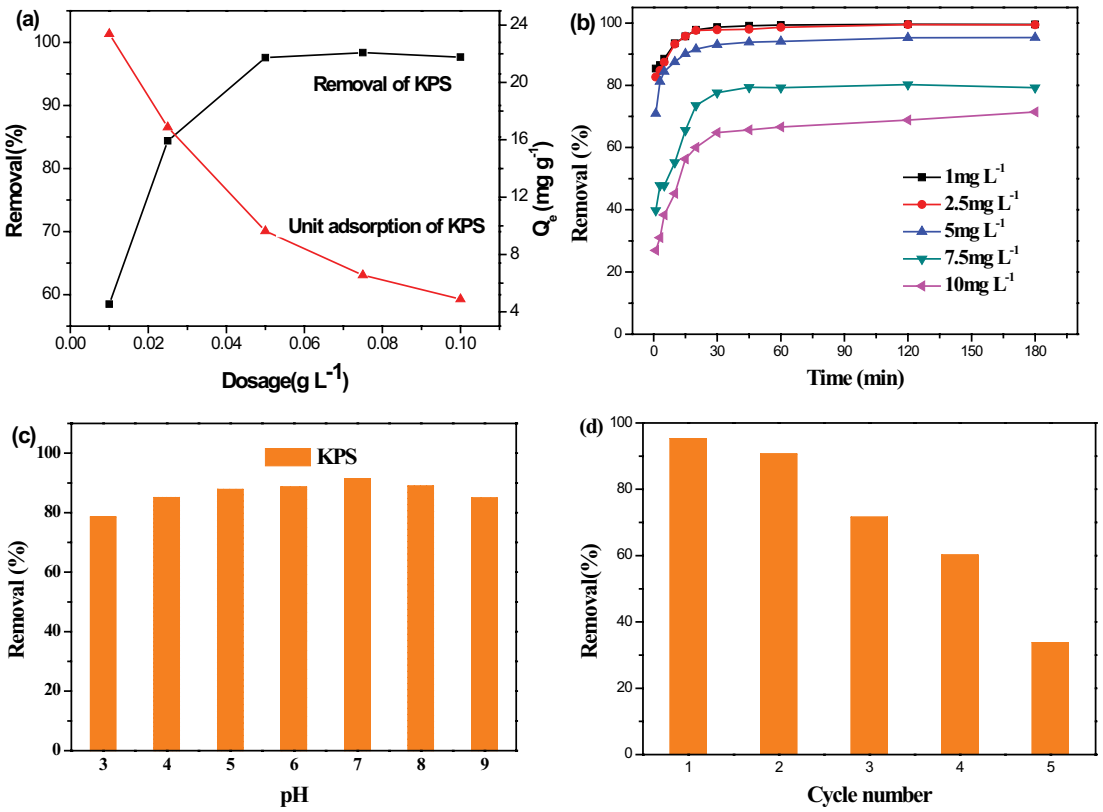

Fig. 6. The influences of operational parameters on ATZ adsorption process: (a) KPS dosage, (b) initial ATZ concentration, (c) solution pH, and (d) stability of KPS. Experimental conditions: $[ATZ]_0$ = 5 mg L^{-1}; [biochar] = 500 mg L^{-1}; pH_0 = 7 ± 0.1.

concentration, the removal efficiency of ATZ also increased gradually. Under the condition of low initial concentration (1–5 mg L^{-1}) within 30 min, the adsorption efficiency of KPS to ATZ could reach 98.67%, 97.82% and 93.05%. At the initial concentration of 7.5 and 10 mg L^{-1}, the removal rate could only reach 77.63% and 64.77%. This is attributed to the increased ATZ concentration which can enhance the adsorption drive between the adsorbent and solute. In addition, when the initial concentration of pollutants in the solution is lower, the time and rate of adsorption to equilibrium is shorter and faster.

3.3.3. Solution pH

Fig. 6c illustrates the effect of solution pH on the ATZ adsorption by KPS. As can be seen from Fig. 6c, the removal rate of ATZ was 78.57%, 85.11%, 87.83%, 88.58%, 91.4%, 88.96% and 84.92% at pH 3–9. The removal rate of ATZ by KPS increased slowly with the increase of pH between 3–7. The maximum adsorption capacity of KPS on ATZ occurred at pH = 7. When the pH value is between 7–9, the removal rate decreases slowly with the increase of pH, and the pH of the initial solution had a weak effect on the adsorption process. For KPS, the point of zero charge (pH_{pzc}) was determined to be 3.70. The surface of KPS was positively charged at pH values below pH_{pzc} and negatively charged above pH_{pzc}. Under acidic conditions, with the increase of pH value, the electron interaction between the positive charge and ATZ ions on the surface of the material is enhanced, thus improving the ATZ. When the pH of the solution is alkaline, most of the materials exist in the state of deprotonation with the reduced form of cation, and the electronegativity around the material weakens the electronic interaction between it and ATZ, so the removal rate of ATZ was reduced. Hence, the ATZ adsorption capacity of KPS was also acceptable under other pH conditions, indicating that KPS will have a strong adaptive energy level in the environment.

3.3.4. Stability of KPS

The reusability of biochar is an important characteristic from the practical viewpoint. To further explore the stability, the KPS was reused for five times under the same condition. It is noted from Fig. 6d that the KPS still had a good adsorption capacity of ATZ at more than 60% within 30 min after four adsorption cycles. The KPS represented well stability, which showed a great potential to be used in the adsorption of ATZ.

3.4. Adsorption kinetics of ATZ

For kinetics study, the adsorption kinetics experiments were conducted through same as above experimental method. The adsorption kinetics was determined using the pseudo-first-order equation, pseudo-second-order equation and the Elovich models. The formula is as follows [33]:

Pseudo-first-order:

$$\ln\left(Q_t - Q_t\right) = \ln Q_e - k_1 t \tag{2}$$

Pseudo-second-order:

$$\frac{t}{Q_e} = \frac{1}{k_2 Q_t^2} + \frac{t}{Q_e} \tag{3}$$

Elovich:

$$Q_t = b\ln\left(ab\right) + b\ln\left(t\right) \tag{4}$$

where Q_t and Q_e represent the amount of ATZ (mg g^{-1}) removed at time t and at equilibrium, respectively; k_1 and k_2 represent the first-order and second-order sorption rate constants (min^{-1}) and (g (mg min)$^{-1}$), respectively; a and b are Elovich coefficients.

The intraparticle diffusion model could be presented as:

$$Q_t = k_q \cdot t^{0.5} + c_1 \tag{5}$$

The liquid film diffusion model could be expressed as:

$$\ln\left(1 - \frac{Q_t}{Q_e}\right) = -k_{\text{fd}} t + c_2 \tag{6}$$

where Q_t, Q_e and t are defined above, k_p (mol g^{-1} $L^{-0.5}$) is the intraparticle diffusion rate constant and k_{fd} (h^{-1}) is the liquid film diffusion rate constant, c_1 and c_2 are the intercepts [37].

The adsorption kinetic curves were fitted by the pseudo-first-order (Fig. 7a) and pseudo-second-order equation (Fig. 7b), and the corresponding kinetic parameters are listed in Table 2. The results show that the R^2 obtained by the pseudo-second-order rate equation ($R^2 > 0.99$) is superior to that obtained by the pseudo-first-order equation. Similar kinetic model fittings were reported for the different adsorbent-pollutant systems in literature [34–36]. The adsorption rate of PS-based biochar on ATZ is proportional to the square of adsorption position, indicating that chemical adsorption is the main reaction. The results also showed that the adsorption of PS-based biochar on ATZ was heterogeneous and followed the binuclear surface adsorption mechanism.

Moreover, the pseudo-second-order kinetic model included all the adsorption processes, such as the internal diffusion, caused by the surface adsorption force and the external liquid film diffusion [37]. Therefore, the ATZ adsorption of the PS-based biochar may be involved with the following adsorption processes: (1) intraparticle diffusion, describing the diffusion within the pores, and (2) film diffusion, describing the diffusion along the surface of the pores [38]. The Eqs. (1) and (2) processes could be proved by the intraparticle model [Eq. (5)] and the liquid film diffusion model [Eq. (6)], respectively. From Fig. 7c and d, the slope of $-\ln(1 - Q_t/Q_e)$ vs. t and the slope of Q_t vs. $t^{0.5}$ both yielded two different linear stages. Complex mathematical relationships differed by geometry and nature of the adsorbent, indicating that ATZ adsorption included both film diffusion and intraparticle diffusion. Furthermore, in the process of the PS-based biochar on ATZ, the model

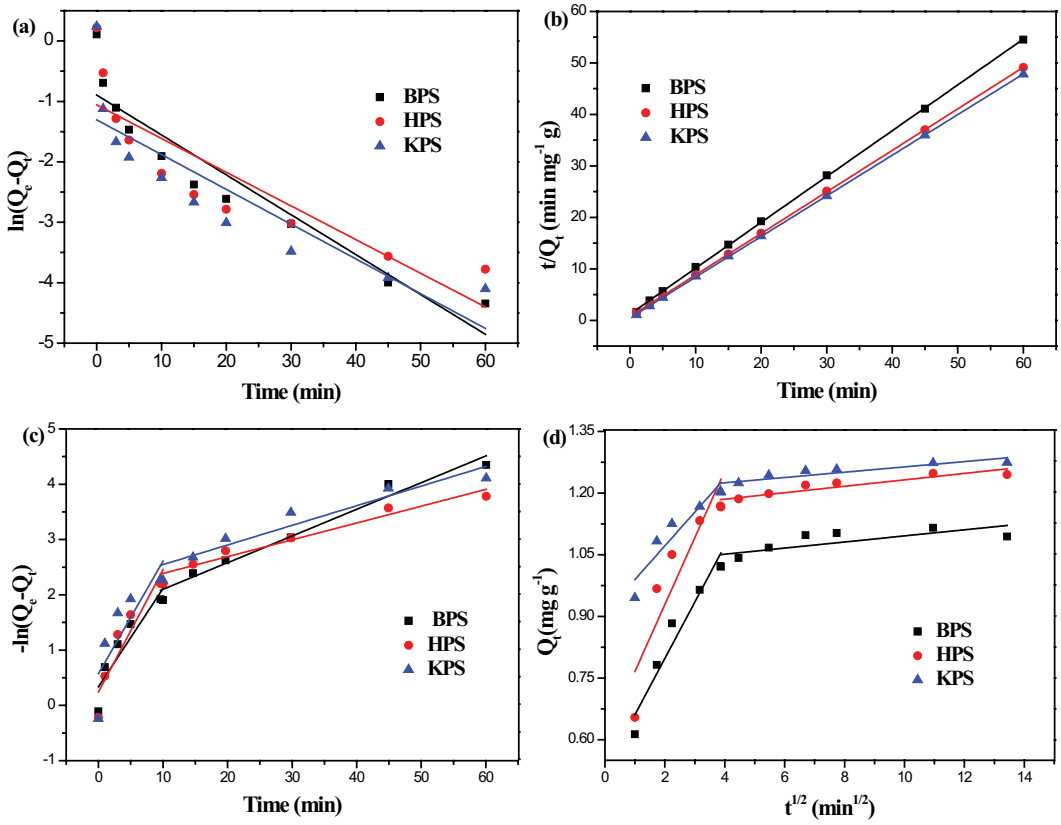

Fig. 7. The ATZ adsorption curve was fitted by a pseudo-first-order kinetic model (a), a pseudo-secondary kinetic model (b), a liquid film diffusion model (c), and kinetic plots of intraparticle diffusion model (d).

Table 2
Kinetic equation parameters of adsorption ATZ of BPS, HPS and KPS

Biochar	C_0 (mg L^{-1})	Experiment Q_e (mg g^{-1})	Pseudo-first-order kinetics model		Pseudo-second-order kinetics model			Elovich model		
			k_1 (min^{-1})	R^2	k_2 (g (mg min)$^{-1}$)	v_0 (g min mg^{-1})	R^2	a (g (mg min)$^{-1}$)	b (g mg^{-1})	R^2
BPS	5	7.94	0.16	0.22	0.58	1.28	0.99	0.06	1.23	0.87
HPS	5	8.96	0.13	0.20	0.44	1.34	0.99	0.02	1.89	0.79
KPS	5	9.70	0.14	0.15	0.59	1.92	0.99	0.09	0.83	0.89

equations of particle diffusion had not passed through the origin, which indicated that intraparticle diffusion wasn't the only decisive process of adsorption rate. As can be seen from Table 2, the Q_e (9.70 mg L^{-1}) of the KPS was larger than the two biochar, and the v_0 was increased from 1.28 (g min) mg^{-1} (BPS) to 1.93 (g min) mg^{-1} (KPS). Therefore, the results illustrated that the KPS represented the best adsorption capacity on ATZ, which is in accordance with the results in Fig. 5.

Above all, the combination of physical adsorption and chemical adsorption is the main mechanism of ATZ adsorption by the PS-based biochar. According to the kinetic model and internal diffusion model results, the adsorption process of biochar for ATZ includes two steps. Firstly, ATZ ions in the solution were adsorbed onto the surface of biochar by electrostatic attraction and chemical bond force (such as π electron and hydrogen bond). Then, most of the ATZ molecules continue to diffuse into the pore structure of the material. Current studies indicate that the main mechanism of pore-filled pesticide adsorption is also the same for ATZ [15]. For BPS and HPS, the adsorption process of ATZ is slower and slower than that of KPS, especially in pores, but the adsorption process is basically the same. The specific surface area of the material was improved by modification of potassium carbonate.

3.5. Adsorption isotherm of ATZ

The adsorption isotherm model is important for describing the adsorption process. The data of adsorption isotherm

Table 3
Adsorption isotherm equation fitting parameters

Biochar	Langmuir equation			Freundlich equation		
	Q_m (mg g^{-1})	b (L mg^{-1})	R^2	n	k (mg$^{1-1/n}$ L$^{1/n}$ g^{-1})	R^2
BPS	8.14	9.65	0.94	3.63	3.19	0.99
HPS	9.22	7.60	0.98	3.23	3.13	0.99
KPS	11.78	42.27	0.96	3.63	3.19	0.99

model is very important for determining the adsorption capacity and describing the surface properties [39]. The adsorption isotherm model was investigated at ATZ solution concentrations ranging from 1 to 10 mg L^{-1}. These isotherm data were treated according to the two well-known isotherm models: Langmuir and Freundlich. The linearized forms of Langmuir and Freundlich isotherm models are given in Eqs. (7) and (8), respectively [33]:

Langmuir:

$$Q_e = \frac{Q_m}{1+bC_e} bQ_e \tag{7}$$

Freundlich:

$$\ln Q_e = \ln k + \ln C_e \tag{8}$$

where Q_e is the equilibrium adsorption capacity (mg g^{-1}); Q_m is saturation adsorption capacity (mg g^{-1}); C_e is the equilibrium adsorption concentration (mg L^{-1}); b is the adsorption equilibrium constant (L mg^{-1}).

Langmuir and Freundlich isothermal adsorption equations were used to fit the experimental data in Table 3. The Freundlich calculation ($R^2 > 0.99$) could well indicate that the adsorption of PS-based biochar to ATZ is multimolecular layer adsorption. Where, if $n > 1$, then the adsorption process was spontaneous. The obtained isotherm results are in agreement with the previous studies [40–42]. As shown in Table 3, n = 3.30, n = 3.23, and n = 3.63 were all greater than 1, indicating that the adsorption process could proceed spontaneously. Moreover, the adsorption conforms to the Freundlich model, which also indicated that the adsorption of the PS-based biochar on ATZ were uneven surface adsorption, and consistent with the material characteristics. Meanwhile, the adsorption capacity of KPS to ATZ was superior to the two biochar and the Q_m was 11.78 mg g^{-1}.

3.6. Adsorption thermodynamics of ATZ

Isothermal adsorption of ATZ at different temperatures (20°C, 25°C, 30°C and 35°C) was investigated using the same procedures above. The adsorption thermodynamics enthalpy change (ΔH^θ) and entropy (ΔS) and the change of Gibb's free energy values (ΔG^θ), formula is as follows [31]:

$$\Delta G^\theta = -RT\ln K_e \tag{9}$$

Table 4
Thermodynamic parameters of ATZ adsorbed by biochar at different temperatures

Adsorbent	T/K	ΔG (kJ mol^{-1})	ΔH (kJ mol^{-1})	ΔS (kJ mol^{-1} K^{-1})
BPS	298	3.74	–19.63	–0.08
	303	4.52		
	308	5.30		
HPS	298	5.18	–21.34	–0.09
	303	6.07		
	308	6.96		
KPS	298	5.82	–43.49	–0.17
	303	7.47		
	308	9.13		

$$\ln K_e = \frac{\Delta S}{R} - \frac{\Delta H}{RT} \tag{10}$$

$$\Delta G = \Delta H - T\Delta S \tag{11}$$

where T is the absolute temperature (K), K_e is the thermodynamic equilibrium constant (based on $\ln(Q_e/C_e)$, and ΔH and ΔS can be obtained by the slope and intercept of $\ln K$ plotted against T^{-1}.

Adsorption thermodynamics could indicate the dynamics and direction of the adsorption process. The adsorption capacity of the adsorbents depends on the number of collisions between the adsorbents and organic pollutants. With the increase of temperature, the adsorption capacity of the PS-based biochar increased to different degrees. Thus, the adsorption of the PS-based biochar on ATZ was endothermic reaction. ΔG^θ of the PS-based biochar (Table 4) was negative, showing the adsorption reaction of ATZ occurred spontaneously, which was consistent with the parameter $n > 1$ in the Freundlich model. The positive ΔH of adsorption reaction indicated that the ATZ adsorption process of materials was endothermic, temperature rise could promote adsorption, also indicated that high temperature was conducive to adsorption.

4. Conclusions

In this study, the adsorption performance of the PS-based biochar obtained via the high-temperature pyrolysis and the hydrothermal activation method were investigated. The characterization results on physicochemical properties exhibited that KPS had optimal specific surface area and pore structure, which could reach 335.27 m^2 g^{-1}, 30.48 Å and 0.26 cm^3 g^{-1}, respectively. Moreover, the KPS had effective adsorption capacity on ATZ, and the Langmuir Q_m could reach 11.78 mg g^{-1} (R^2 = 0.998). Various operating conditions such as adsorbent dose, the effect of pH, and initial ion concentration studies suggested that the highest ATZ removal occurred at an initial ion concentration of 5 mg L^{-1} at pH 7.0 with an adsorbent dose of 0.5 g L^{-1}. The adsorption process was better fitted with pseudo-second-order kinetic model and Freundlich

model. It indicated that the adsorption of the PS-based biochar on ATZ was a multi-molecular layer adsorption process dominated by chemical adsorption. The adsorption of the PS-based biochar on ATZ was endothermic reaction and could proceed spontaneously. Furthermore, the KPS maintained the high activity and stability after five times cycling experiments. Moreover, the PS-based biochar were designed as efficient adsorbents for organic pollutants removal as well as a new application approach for the resource utilization of agricultural wastes.

Recommendations for future research

- Adsorption study of by biochar on dyes, heavy metals and other organic pollutants.
- Using the produced adsorbent as a pilot in industrial wastewater and its practical application.
- Recycling more waste resources for water purification.

Declaration of competing interest

The authors do not have any conflict of interests to declare.

Acknowledgement

This work was financially supported by the National Natural Science Foundation of China (No. 51808412), the Natural Science Foundation of Hubei province (No. 2018CFB266), and the Central Government Guidance for Local Science and Technology Development Projects of Hubei province (No. 2019ZYYD068).

References

[1] J. Jin, M.J. Kang, K. Sun, Z.Z. Pan, F.C. Wu, B.S. Xing, Properties of biochar-amended soils and their sorption of imidacloprid, isoproturon, and atrazine, Sci. Total Environ., 550 (2016) 504–513.
[2] Y.C. Hong, J.L. Peng, X.G. Zhao, Y. Yan, B. Lai, G. Yao, Efficient degradation of atrazine by CoMgAl layered double oxides catalyzed peroxymonosulfate: optimization, degradation pathways and mechanism, Chem. Eng. J., 370 (2019) 354–363.
[3] J.T. Sanderson, W. Seinen, J.P. Giesy, M.V.D. Berg, 2-Chloro-s-triazine herbicides induce Aromatase (CYP19) activity in H295R human adrenocortical carcinoma cells a novel mechanism for estrogenicity, Toxicol. Sci., 54 (2000) 121–127.
[4] T.B. Hayes, A. Collins, M. Lee, M. Mendoza, N. Noriega, A.A. Stuart, A. Vonk, Hemaphroditic, denasculinized frogs after exposure to the herbicide atrazine at low ecologically relevant doses, Proc. Natl. Acad. Sci. U.S.A., 99 (2002) 5476–5480.
[5] Q. Huang, S. Song, Z. Chen, B.W. Hu, J.R. Chen, X.K. Wang, Biochar-based materials and their applications in removal of organic contaminants from wastewater: state-of-the-art review, Biochar, 1 (2019) 45–73.
[6] A. Dutta, N. Singh, Surfactant-modified bentonite clays: preparation, characterization, and atrazine removal, Environ. Sci. Pollut. Res. Int., 22 (2015) 3876–3885.
[7] Z.C. Yang, A.Q. Yu, C. Shan, G.D. Gao, B.C. Pan, Enhanced Fe(III)-mediated Fenton oxidation of atrazine in the presence of functionalized multi-walled carbon nanotubes, Water Res., 137 (2018) 37–46.
[8] Y.T. Han, X. Cao, X. Ouyang, S.P. Sohi, J.W. Chen, Adsorption kinetics of magnetic biochar derived from peanut hull on removal of Cr(VI) from aqueous solution: effects of production conditions and particle size, Chemosphere, 145 (2016) 336–341.
[9] M. Ahmad, S.S. Lee, X.M. Dou, D. Mohan, J.K. Sung, J.E. Yang, Y.S. Ok, Effects of pyrolysis temperature on soybean stover- and peanut shell-derived biochar properties and TCE adsorption in water, Bioresour. Technol., 118 (2012) 536–544.
[10] L.C. Zhou, J.J. Ma, H. Zhang, Y.M. Shao, Y.F. Li, Fabrication of magnetic carbon composites from peanut shells and its application as a heterogeneous Fenton catalyst in removal of methylene blue, Appl. Surf. Sci., 324 (2015) 490–498.
[11] H.Q. Li, S.J. Liu, S.W. Qiu, L. Sun, X.J. Yuan, D.S. Xia, Catalytic ozonation oxidation of ketoprofen by peanut shell-based biochar: effects of the pyrolysis temperatures, Environ Technol., 43 (2020) 1–13.
[12] Z.B. Pan, Y.M. Lin, B. Sarkar, G. Owens, Z.L. Chen, Green synthesis of iron nanoparticles using red peanut skin extract: synthesis mechanism, characterization and effect of conditions on chromium removal, J. Colloid Interface Sci., 558 (2020) 106–114.
[13] Z.B. Pan, Y.M. Lin, B. Sarkar, G. Owens, Z.L. Chen, Green synthesis of iron nanoparticles using red peanut skin extract: synthesis mechanism, characterization and effect of conditions on chromium removal, J. Colloid Interface Sci., 558 (2020) 106–114.
[14] J.W. Yang, G.Z. Ji, Y. Gao, W. Fu, M. Irfan, L. Mu, Y.L. Zhang, A.M. Li, High-yield and high-performance porous biochar produced from pyrolysis of peanut shell with low-dose ammonium polyphosphate for chloramphenicol adsorption, J. Cleaner Prod., 264 (2020) 121516, doi: 10.1016/j.jclepro.2020.121516.
[15] R.A. Yokley, M.W. Cheung, Analytical method for the determination of atrazine and its dealkylated chlorotriazine metabolites in water using gas chromatography mass selective detection, J. Agric. Food Chem., 48 (2000) 4500−4507.
[16] X. Xu, S.L. Yu, W.X. Shi, Z.Q. Jiang, C. Wu, Effect of acid medium on the coagulation efficiency of polysilicate-ferric (PSF)—a new kind of inorganic polymer coagulant, Sep. Purif. Technol., 66 (2009) 486–491.
[17] Z.G. Liu, F.S. Zhang, J.Z. Wu, Characterization and application of chars produced from pinewood pyrolysis and hydrothermal treatment, Fuel, 89 (2010) 510–514.
[18] X.P. Bai, G.H. Wang, C.X. Gong, Y. Yu, W.N. Liu, D.C. Wang, Co-pelletizing characteristics of torrefied wheat straw with peanut shell, Bioresour. Technol., 233 (2017) 373–381.
[19] M.J. Kim, S.W. Choi, H.W. Kim, S.Y. Mun, K.B. Lee, Simple synthesis of spent coffee ground-based microporous carbons using K_2CO_3 as an activation agent and their application to CO_2 capture, Chem. Eng. J., 397 (2020) 125404, doi: 10.1016/j.cej.2020.125404.
[20] Y.Q. Chen, H.P. Yang, X.H. Wang, S.H. Zhang, H.P. Chen, Biomass-based pyrolytic polygeneration system on cotton stalk pyrolysis: influence of temperature, Bioresour. Technol., 107 (2012) 411–418.
[21] Y.B. Xi, Y.Y. Wang, D.J. Yang, Z.K. Zhang, W.L. Liu, Q. Li, X.Q. Qiu, K_2CO_3 activation enhancing the graphitization of porous lignin carbon derived from enzymatic hydrolysis lignin for high performance lithium-ion storage, J. Alloys Compd., 785 (2019) 706–714.
[22] J. Wang, S. Kaskel, KOH activation of carbon-based materials for energy storage, J. Mater. Chem., 22 (2012) 23710–23725.
[23] M.I. Al-Wabel, A. Al-Omran, A.H. El-Naggar, M. Nadeem, A.R. Usman, Pyrolysis temperature induced changes in characteristics and chemical composition of biochar produced from conocarpus wastes, Bioresour. Technol., 131 (2013) 374–379.
[24] S.L. Zhang, L.C. Tao, Y.L. Zhang, Z.K. Wang, G.J. Gou, M. Jiang, C.P. Huang, Z.W. Zhou, The role and mechanism of K_2CO_3 and Fe_3O_4 in the preparation of magnetic peanut shell based activated carbon, Powder Technol., 295 (2016) 152–160.
[25] P. Zhang, D. O'Connor, Y.N. Wang, L. Jiang, T.X. Xia, L.W. Wang, D.C.W. Tsang, Y.S. Ok, D. Hou, A green biochar/iron oxide composite for methylene blue removal, J. Hazard. Mater., 384 (2020) 121286, doi: 10.1016/j.jhazmat.2019.121286.
[26] E.R.C. Coelho, G.M. Brito, L.F. Loureiro, M.A. Schettino Jr., J.C.C.D. Freitas, 2,4-dichlorophenoxyacetic acid (2,4-D)

micropollutant herbicide removing from water using granular and powdered activated carbons: a comparison applied for water treatment and health safety, J. Environ. Sci. Health., Part B, 55 (2020) 361–375.
[27] X.R. Jing, Y.Y. Wang, W.J. Liu, Y.K. Wang, H. Jiang, Enhanced adsorption performance of tetracycline in aqueous solutions by methanol-modified biochar, Chem. Eng. J., 248 (2014) 168–174.
[28] H.H. Lyu, J.C. Tang, Y. Huang, L.S. Gai, E.Y. Zeng, K. Liber, Y.Y. Gong, Removal of hexavalent chromium from aqueous solutions by a novel biochar supported nanoscale iron sulfide composite, Chem. Eng. J., 322 (2017) 516–524.
[29] H.H. Lyu, Y.Y. Gong, J.S. Tang, Y. Huang, Q.L. Wang, Immobilization of heavy metals in electroplating sludge by biochar and iron sulfide, Environ. Sci. Pollut. Res. Int., 23 (2016) 14472–14488.
[30] M. Messaoudi, M. Douma, N. Tijani, Y. Dehmani, L. Messaoudi, Adsorption process of the malachite green onto clay: kinetic and thermodynamic studies, Desal. Water Treat., 240 (2021) 191–202.
[31] Y.S. Ho, J. Ng, G. McKay, Kinetics of pollutant sorption by biosorbents: review, ChemInform, 29 (2010) 189–232.
[32] H. Qiu, L. Lv, B.C. Pan, Q.J. Zhang, W.M. Zhang, Q.X. Zhang, Critical review in adsorption kinetic models, J. Zhejiang Univ.-Sci. A, 10 (2009) 716–724.
[33] M. Yousefi, M. Gholami, V. Oskoei, A.A. Mohammadi, M. Baziar, A. Esrafili, Comparison of LSSVM and RSM in simulating the removal of ciprofloxacin from aqueous solutions using magnetization of functionalized multi-walled carbon nanotubes: process optimization using GA and RSM techniques, J. Environ. Chem. Eng., 9 (2021) 105677, doi: 10.1016/j.jece.2021.105677.
[34] O. Duman, C. Özcan, T.G. Polat, S. Tunc, Carbon nanotube-based magnetic and non-magnetic adsorbents for the high-efficiency removal of diquat dibromide herbicide from water: omwcnt, omwcnt-Fe_3O_4 and omwcnt-κ-carrageenan-Fe_3O_4 nanocomposites, Environ. Pollut., 244 (2019) 723–732.
[35] E. Ayranci, O. Duman, In-situ UV-visible spectroscopic study on the adsorption of some dyes onto activated carbon cloth, Sep. Sci. Technol., 44 (2009) 3735–3752.
[36] O. Duman, E. Ayranci, Adsorptive removal of cationic surfactants from aqueous solutions onto high-area activated carbon cloth monitored by in situ UV spectroscopy, J. Hazard. Mater., 174 (2010) 359–367.
[37] B.L. Chen, D.D. Zhou, L.Z. Zhu, Transitional adsorption and partition of nonpolar, Environ. Sci. Technol., 42 (2008) 5137–5143.
[38] K.B. Petrotos, P.E. Gkoutsidis, M.I. Kokkora, K.G. Giankidou, A.G. Tsagkarelis, A study on the kinetics of olive mill wastewater (OMWW) polyphenols adsorption on the commercial XAD4 macroporous resin, Desal. Water Treat., 51 (2013) 2021–2029.
[39] Y. Ding, D.B. Jing, H.L. Gong, L.B. Zhou, X.S. Yang, Biosorption of aquatic cadmium(II) by unmodified rice straw, Bioresour. Technol., 114 (2012) 20–25.
[40] E. Ayranci, O. Duman, Adsorption behaviors of some phenolic compounds onto high specific area activated carbon cloth, J. Hazard. Mater., 124 (2005) 125–132.
[41] O. Duman, E. Ayranci, Structural and ionization effects on the adsorption behaviors of some anilinic compounds from aqueous solution onto high-area carbon-cloth, J. Hazard. Mater., 120 (2005) 173–181.
[42] E. Ayranci, O. Duman, Removal of anionic surfactants from aqueous solutions by adsorption onto high area activated carbon cloth studied by in situ UV spectroscopy, J. Hazard. Mater., 148 (2007) 75–82.